Provided for non-commercial research and educational use only.
Not for reproduction or distribution or commercial use.

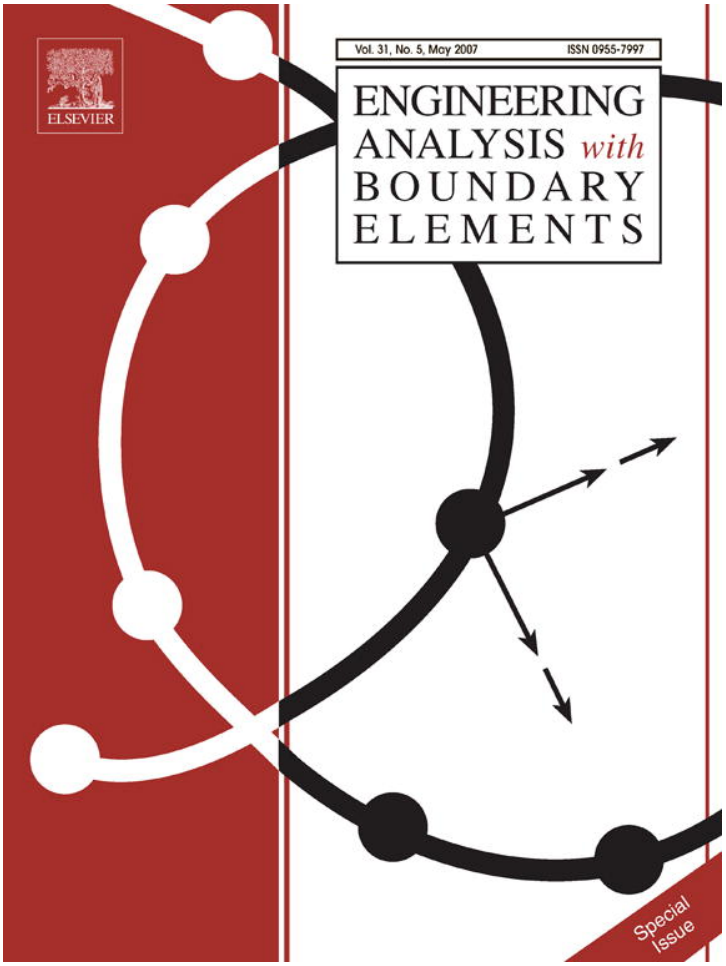

This article was originally published in a journal published by Elsevier, and the attached copy is provided by Elsevier for the author's benefit and for the benefit of the author's institution, for non-commercial research and educational use including without limitation use in instruction at your institution, sending it to specific colleagues that you know, and providing a copy to your institution's administrator.

All other uses, reproduction and distribution, including without limitation commercial reprints, selling or licensing copies or access, or posting on open internet sites, your personal or institution's website or repository, are prohibited. For exceptions, permission may be sought for such use through Elsevier's permissions site at:

http://www.elsevier.com/locate/permissionusematerial

ELSEVIER

Engineering Analysis with Boundary Elements 31 (2007) 388–401

ENGINEERING ANALYSIS with BOUNDARY ELEMENTS

www.elsevier.com/locate/enganabound

Systematic study of thermal properties of CNT composites by the fast multipole hybrid boundary node method

Jianming Zhang*, Masataka Tanaka

Department of Mechanical Systems Engineering, Shinshu University, 4-17-1 Wakasato, Nagano 380-8553, Japan

Received 7 February 2006; accepted 5 July 2006
Available online 9 February 2007

Abstract

Carbon nanotubes (CNTs) are predicted to possess superior heat conductivity, which makes the CNTs promising in development of fundamentally new composite material. With the current advancement in nanotechnology, it is possible to design materials with desired properties for specific applications. On the other hand, the overall properties of CNT composites are usually evaluated using a representative volume element (RVE) with a number of CNTs embedded. For realistic modeling, an RVE including a large number of CNTs, for example, tens or hundreds, is necessary. However, analysis of such an RVE using standard numerical methods faces two severe difficulties: discretization of the geometry into elements and the very large computational scale. In this paper, the first difficulty is alleviated by developing the hybrid boundary node method (HdBNM), which is a boundary-type meshless method. To overcome the second difficulty, a simplified mathematical model for thermal analysis of CNT analysis is first proposed, by which the size of the linear system can be reduced by nearly half. Then, the HdBNM is combined with the Fast Multipole Method (FMM) based on the model to further reduce the computational scale. A variety of RVEs containing different numbers of CNTs, from small to large scales, have been studied in an attempt to investigate the influence of CNT length, distribution, orientation and volume fraction on the overall thermal properties of the composites. Insights have been gained into the thermal behavior of the CNT composite material.
© 2007 Elsevier Ltd. All rights reserved.

Keywords: Carbon nanotube; Nanocomposites; Heat conductivity; Hybrid boundary node method; Simplified model; Fast Multipole Method

1. Introduction

Since their discovery over a decade ago, carbon nanotubes (CNT) have been attracting considerable attentions both from scientists and engineers. Due to their near-perfect nanostructure, which can be thought of as a hexagonal sheet of carbon atoms rolled into a seamless cylinder with two semi-sphere caps at each end, the CNTs are predicted to possess exceptional physical properties, such as superior heat and electrical conductivities, as well as high stiffness, strength and resilience [1–5]. A few experiments have been reported on mats of compressed ropes of CNTs [6,7]. By assuming that both thermal and electrical conductivities follow the same rules for transport, values of thermal conductivity of CNTs, ranging from 1750 to 5850 W/m K, have been extrapolated from experimental measurement on mats of nanotube ropes. The direct measurements of individual nanotube were also performed using MEMS measurement technology [8]. Following those experiments, several preliminary molecular dynamics (MD) simulations [9–11] of the thermal conductivity gave even higher values, i.e., 6600 W/m K at 300 K [9]. Although the estimated values of thermal conductivity were different from each other, it is generally accepted that the CNTs possess excellent heat conductivity, comparable or even higher than diamond. The latter has been considered so far as the best heat conductor.

These remarkable properties may make CNTs ideal for a wide range of technological applications. One of the most intriguing applications is the use of CNTs, as small volume fraction filler, in nanotube-reinforced polymers. CNT-based composites offer significant improvements to structural properties over their base

*Corresponding author. Tel.: +81 26 269 5123; fax: +81 26 269 5124.
E-mail address: zhangjm@homer.shinshu-u.ac.jp (J. Zhang).

0955-7997/$ - see front matter © 2007 Elsevier Ltd. All rights reserved.
doi:10.1016/j.enganabound.2006.07.011

Author's personal copy

polymers. It has been demonstrated that with only 1% (weight fraction) of CNTs added to a matrix material, the stiffness of a resulting composite can increase as high as 36–42% and the tensile strength up to 25% [12]. In the work of Biercuk et al. [13], samples of industrial epoxy loaded with 1 wt% SWNTs showed a 70% increase in heat conductivity at 40 K, and rose to 125% at room temperature.

Numerical simulations can help to understand the relationship between the geometrical characteristic (e.g. nanotube orientation) and the properties of the nanocomposites. This will allow the determination and optimization of different processing method to manufacture the nanocomposite materials. At the nanoscale level, atomistic or MD somehow appears a "natural" simulation method, and has provided abundant results helping in understanding their thermal, mechanical and electrical behaviors. However, due to the limitations in current computing power, these simulations are so far limited to single pure CNT or very small scales for CNT-composite, for example, an representative volume element (RVE) including single short CNT, only. To study the influence of CNTs distribution on the effective properties of the composite, modeling of an RVE including a large number of CNTs that are randomly distributed and oriented is necessary. This is because, in a real CNT-composite, the CNTs are not uniform in size and shape. They can be straight, twisted and curled or in the form of ropes and their distribution and orientation in the matrix can be nonuniform, unidirectional or random. Even with the most superior computer resources available in the world, computation of such an RVE by MD is almost impossible. Liu et al. [14] have demonstrated that the use of atomistic or MD simulations is inevitable for the analysis of such nanomaterials in order to study the local load transfers, interface properties, or failure modes at the nanoscale. However, for the global analysis studying the effects of CNTs configuration on the overall properties of the material, they suggested a continuum model, in which the physical behavior of the composite is governed by continuum equations such as Laplace's equation for thermal property and Lame–Navier equations for elastic properties. Sohlberg et al. [15] have discussed the application of continuum mechanics to nanostructural engineering, and demonstrated by numerical results that methods of continuum mechanics provide a viable and efficient alternative to the standard methods for vibration analysis of nanotubes.

The aim of this study is to gain insight into the thermal properties of CNT-based composites through numerical simulation based on continuum formulation. The effective heat conductivity of CNT-based composites is evaluated using a RVE based on 3-D potential theory. In the RVE, a single/multiple nanotube(s) with surrounding matrix material are modeled, with properly applied boundary and interface conditions to account for the effects of the surrounding materials.

The most critical part of any numerical analysis is the discretization of domain of interest. If the domain contains thin-walled structures of complex geometry (e.g. twisted, curved, randomly distributed), the task of its proper/high quality meshing is always challenging. An implementation of Finite Element Method (FEM) to the modeling of such types of structures results in extremely large number of elements, due to obvious restriction of element connectivity and requirements of appropriate values of their aspect ratios. The Boundary Element Method (BEM) based models partially alleviate the problem, as the discretization of boundary surfaces (instead of volumes) is required, only. However, still in many cases the high quality boundary elements may be difficult and cumbersome to obtain. To overcome meshing problems, a meshless method can be used, for example, the hybrid boundary node method (HdBNM) [16–20] or others [21–23]. By combining a modified functional with the moving least squares (MLS) approximation, the HdBNM is a truly meshless, boundary-only method. The HdBNM requires only the discrete nodes located on the surface of the domain and, hence, considerably simplifies the discretization task and leads to substantial resources savings.

Another difficulty in the analysis is that the computational scale may be extremely large exceeding the current computer power. Due to the very thin and slender structure of the CNTs, a large number of nodes are required to discretize them in order to capture the steep gradients. Moreover, in a multi-domain solver, at each node on the interface of a CNT with the host polymer, both temperature and normal flux are unknown. This situation considerably increases the total degrees of freedom in the overall system of equations. Our preliminary studies have shown that temperatures within the entire CNT are almost uniform due to the huge difference of heat conductivity between the CNT and the host polymer [24]. Based on this observation, we have proposed a simplified mathematical model, where the CNTs are considered as heat superconductors and uniform temperature distributions within the entire body of each CNT assumed [25]. As a result, the total number of degrees of freedom is reduced by nearly half, and thus increases the number of CNTs contained in an RVE that can be analyzed within available computer resources. The simplified model has been rigorously tested and validated using benchmark examples.

Nevertheless, even with the simplified model, both the memory requirements and the computational scale are still of $O(N^2)$ when an iterative solver is applied. Under the use of a direct solver, the Gaussian elimination, for example, the computational scale is even higher up to $O(N^3)$, where N stands for the total number of degrees of freedom. To perform analysis of a real-world RVE model, an efficient technique further reducing computational requirements is necessary. The method of choice is Fast Multipole Method (FMM).

Author's personal copy

The FMM was introduced by Rokhlin [26], and developed by Greengard [27–29] as an algorithm for the rapid evaluation of Coulombic interactions in a large-scale ensemble of particles. In their method, multipole moments are used to represent distant particle groups, a local expansion to evaluate the contribution from distant particles in the form of a series, and a hierarchical decomposition of the domain to carry out efficient and systematic grouping of the particles. The FMM reduces both memory size and computational scale from $O(N^2)$ to $O(N)$, thus enabling scientific and engineering computations that were previously impossible.

The FMM has been applied to a variety of computation methods. Applying FMM to accelerate BEM computation has been investigated by many researchers [30–34], and the computational costs of the fast BEM, including memory and CPU time, have been successfully reduced to $O(N)$. Recently, we have combined the FMM with the HdBNM [35], and derived an efficient algorithm in terms of both computer and human-labor costs.

In this paper, we first combine the HdBNM with a multi-domain solver and apply the combined approach to perform some preliminary computations and investigate the influences of the CNT length and dispersion on the effective thermal properties of the composites. Then we present the full formulation of the simplified mathematical model for simulation of thermal behavior of CNT-based composites. The FMM techniques are used to accelerate the solution process of the established linear system of equations. The above algorithms and mathematical model are implemented into a computer code written in C++ and employed for advanced simulations, where the RVEs contain a number of CNTs with a variety of lengths, shapes, distribution and orientation. An effective shape of the CNT that significantly increases the effective heat conductivity of the composites is found. Finally, we perform some sensitive studies investigating the impact of CNT's curvature upon the effectiveness of reinforcement. It is also demonstrated that the HdBNM accelerated with the FMM is very promising for large-scale analysis of fiber-reinforced composites.

2. Multi-domain modeling of CNT composites

A multi-domain formulation is a natural way to model inclusion problems. However, thermal analysis of the CNT composites using standard numerical solution techniques like FEM or BEM faces severe difficulties in discretization of the domain geometry. In this work, this difficulty is alleviated by employing HdBNM, which is a meshless, boundary-only method and requires only discrete nodes located on the surface of the domain and its parametric representation. As the parametric representation of created geometry is used in all CAD packages, it should be possible to exploit their *Open Architecture* features and handle truly arbitrary geometry. In this section, formulations for the multi-domain HdBNM are derived. For full details of single domain HdBNM for 3-D potential problems refer to [20].

Suppose that n CNTs are distributed in a polymer matrix that makes an RVE. It is assumed that both the CNTs and the matrix in the RVE are continua of linear, isotropic and homogenous materials with given heat conductivities. A steady-state heat conduction problem governed by Laplace's equation with proper boundary conditions is considered for each CNT domain and the matrix domain.

The HdBNM is based on a modified variational principle, in which there are three independent variables, namely:

- temperature within the domain, ϕ;
- boundary temperature, $\tilde{\phi}$;
- boundary normal heat flux, $\tilde{q}$.

Suppose that N nodes are randomly distributed on the bounding surface of a single domain. The domain temperature is approximated using fundamental solutions as follows:

$$\phi = \sum_{I=1}^{N} \phi_I^s x_I \tag{1}$$

and hence at a boundary point, the normal heat flux is given by

$$q = -\kappa \sum_{I=1}^{N} \frac{\partial \phi_I^s}{\partial n} x_I, \tag{2}$$

where ϕ_I^s is the fundamental solution with the source at a node $\mathbf{s}_I$, κ is the heat conductivity and x_I are unknown parameters. For 3-D steady-state heat conduction problems, the fundamental solution can be written as

$$\phi_I^s = \frac{1}{\kappa} \frac{1}{4\pi r(Q, \mathbf{s}_I)}, \tag{3}$$

where Q is a field point; $r(Q, \mathbf{s}_I)$ is the distance between Q and $\mathbf{s}_I$.

The boundary temperature and normal heat flux are interpolated by the MLS [20]:

$$\tilde{\phi}(\mathbf{s}) = \sum_{I=1}^{N} \Phi_I(\mathbf{s}) \hat{\phi}_I \tag{4}$$

and

$$\tilde{q}(\mathbf{s}) = \sum_{I=1}^{N} \Phi_I(\mathbf{s}) \hat{q}_I. \tag{5}$$

In the foregoing equations, $\Phi_I(\mathbf{s})$ is the shape function of MLS approximation; $\hat{\phi}_I$ and $\hat{q}_I$ are nodal values of temperature and normal flux, respectively.

Author's personal copy

For the polymer domain, the following set of HdBNM equations can be written:

$$\begin{bmatrix} \boldsymbol{U}_{00}^p & \boldsymbol{U}_{01}^p & \cdots & \boldsymbol{U}_{0n}^p \\ \boldsymbol{U}_{10}^p & \boldsymbol{U}_{11}^p & \cdots & \boldsymbol{U}_{1n}^p \\ \vdots & \vdots & \ddots & \vdots \\ \boldsymbol{U}_{n0}^p & \boldsymbol{U}_{n1}^p & \cdots & \boldsymbol{U}_{nn}^p \end{bmatrix} \begin{Bmatrix} \boldsymbol{x}_0^p \\ \boldsymbol{x}_1^p \\ \vdots \\ \boldsymbol{x}_n^p \end{Bmatrix} = \begin{Bmatrix} \boldsymbol{H}_0^p \boldsymbol{\phi}_0^p \\ \boldsymbol{H}_1^p \hat{\boldsymbol{\phi}}_1^p \\ \vdots \\ \boldsymbol{H}_n^p \hat{\boldsymbol{\phi}}_n^p \end{Bmatrix}, \tag{6}$$

$$\begin{bmatrix} \boldsymbol{V}_{00}^p & \boldsymbol{V}_{01}^p & \cdots & \boldsymbol{V}_{0n}^p \\ \boldsymbol{V}_{10}^p & \boldsymbol{V}_{11}^p & \cdots & \boldsymbol{V}_{1n}^p \\ \vdots & \vdots & \ddots & \vdots \\ \boldsymbol{V}_{n0}^p & \boldsymbol{V}_{n1}^p & \cdots & \boldsymbol{V}_{nn}^p \end{bmatrix} \begin{Bmatrix} \boldsymbol{x}_0^p \\ \boldsymbol{x}_1^p \\ \vdots \\ \boldsymbol{x}_n^p \end{Bmatrix} = \begin{Bmatrix} \boldsymbol{H}_0^p \hat{\boldsymbol{q}}_0^p \\ \boldsymbol{H}_1^p \hat{\boldsymbol{q}}_1^p \\ \vdots \\ \boldsymbol{H}_n^p \hat{\boldsymbol{q}}_n^p \end{Bmatrix}, \tag{7}$$

where superscript p represents the polymer; subscript 0 stands for the quantities exclusively associated with the polymer domain, and k, $k = 1, \ldots, n$, for the quantities associated with the interface between the kth CNT and the polymer. The sub-matrices $[\boldsymbol{U}]$, $[\boldsymbol{V}]$ and $[\boldsymbol{H}]$ are given as

$$U_{IJ} = \int_{\Gamma_s^J} \phi_I^s v_J(Q) \mathrm{d}\Gamma, \tag{8}$$

$$V_{IJ} = \int_{\Gamma_s^J} q_I^s v_J(Q) \mathrm{d}\Gamma, \tag{9}$$

$$H_{IJ} = \int_{\Gamma_s^J} \Phi_I(\mathbf{s}) v_J(Q) \mathrm{d}\Gamma, \tag{10}$$

where Γ_s^J is a regularly shaped local region around a given node $\mathbf{s}_J$, v_J is a weight function and s is a field point on the boundary.

Similarly, for the kth CNT domain, we have

$$\begin{bmatrix} \boldsymbol{U}_{00}^{t_k} & \boldsymbol{U}_{0i}^{t_k} \\ \boldsymbol{U}_{i0}^{t_k} & \boldsymbol{U}_{ii}^{t_k} \end{bmatrix} \begin{Bmatrix} \boldsymbol{x}_0^{t_k} \\ \boldsymbol{x}_i^{t_k} \end{Bmatrix} = \begin{Bmatrix} \boldsymbol{H}_0^{t_k} \hat{\boldsymbol{\phi}}_0^{t_k} \\ \boldsymbol{H}_i^{t_k} \hat{\boldsymbol{\phi}}_i^{t_k} \end{Bmatrix} \tag{11}$$

and

$$\begin{bmatrix} \boldsymbol{V}_{00}^{t_k} & \boldsymbol{V}_{0i}^{t_k} \\ \boldsymbol{V}_{i0}^{t_k} & \boldsymbol{V}_{ii}^{t_k} \end{bmatrix} \begin{Bmatrix} \boldsymbol{x}_0^{t_k} \\ \boldsymbol{x}_i^{t_k} \end{Bmatrix} = \begin{Bmatrix} \boldsymbol{H}_0^{t_k} \hat{\boldsymbol{q}}_0^{t_k} \\ \boldsymbol{H}_i^{t_k} \hat{\boldsymbol{q}}_i^{t_k} \end{Bmatrix}, \tag{12}$$

where the superscript t_k stands for the kth CNT and the subscript i indicates the quantities associated with the interface between the kth CNT and the matrix.

At the interface between a CNT and the polymer both the temperature and heat fluxes must be continuous, i.e.

$$\{\boldsymbol{\phi}_k^p\} = \{\boldsymbol{\phi}_i^{t_k}\} \tag{13}$$

and

$$\{\boldsymbol{q}_k^p\} = -\{\boldsymbol{q}_i^{t_k}\}. \tag{14}$$

Using the continuity conditions, Eqs. (6), (7), (11) and (12) can be assembled into the following expression:

$$\begin{bmatrix} \boldsymbol{A}_{00}^p & \boldsymbol{A}_{01}^p & \boldsymbol{0} & \boldsymbol{0} & \cdots & \boldsymbol{A}_{0k}^p & \boldsymbol{0} & \boldsymbol{0} \\ \boldsymbol{U}_{10}^p & \boldsymbol{U}_{11}^p & -\boldsymbol{U}_{ii}^{t_1} & -\boldsymbol{U}_{i0}^{t_1} & \cdots & \boldsymbol{U}_{1k}^p & \boldsymbol{0} & \boldsymbol{0} \\ \boldsymbol{V}_{10}^p & \boldsymbol{V}_{11}^p & \boldsymbol{V}_{ii}^{t_1} & \boldsymbol{V}_{i0}^{t_1} & \cdots & \boldsymbol{V}_{1k}^p & \boldsymbol{0} & \boldsymbol{0} \\ \boldsymbol{0} & \boldsymbol{0} & \boldsymbol{A}_{0i}^{t_1} & \boldsymbol{A}_{00}^{t_1} & \cdots & \boldsymbol{0} & \boldsymbol{0} & \boldsymbol{0} \\ \vdots & \vdots & \vdots & \vdots & \ddots & \vdots & \vdots & \vdots \\ \boldsymbol{U}_{n0}^p & \boldsymbol{U}_{n1}^p & \boldsymbol{0} & \boldsymbol{0} & \cdots & \boldsymbol{U}_{nn}^p & -\boldsymbol{U}_{ii}^{t_n} & -\boldsymbol{U}_{i0}^{t_n} \\ \boldsymbol{V}_{n0}^p & \boldsymbol{V}_{n1}^p & \boldsymbol{0} & \boldsymbol{0} & \cdots & \boldsymbol{V}_{nn}^p & \boldsymbol{V}_{ii}^{t_n} & \boldsymbol{V}_{i0}^{t_n} \\ \boldsymbol{0} & \boldsymbol{0} & \boldsymbol{0} & \boldsymbol{0} & \cdots & \boldsymbol{0} & \boldsymbol{A}_{0i}^{t_n} & \boldsymbol{A}_{00}^{t_n} \end{bmatrix} \times \begin{Bmatrix} \boldsymbol{x}_0^p \\ \boldsymbol{x}_1^p \\ \boldsymbol{x}_i^{t_1} \\ \boldsymbol{x}_0^{t_1} \\ \vdots \\ \boldsymbol{x}_n^p \\ \boldsymbol{x}_i^{t_n} \\ \boldsymbol{x}_0^{t_n} \end{Bmatrix} = \begin{Bmatrix} \boldsymbol{H}_0^p \boldsymbol{d}_0^p \\ \boldsymbol{0} \\ \boldsymbol{0} \\ \boldsymbol{H}_0^{t_1} \boldsymbol{d}_0^{t_1} \\ \vdots \\ \boldsymbol{0} \\ \boldsymbol{0} \\ \boldsymbol{H}_0^{t_n} \boldsymbol{d}_0^{t_n} \end{Bmatrix}, \tag{15}$$

where $[\boldsymbol{A}_{0k}^*]$, $k = 0, 1, \ldots, n$ and i, and $\{\boldsymbol{d}_0^*\}$ (* represents p or t_k) are formed by merging $[\boldsymbol{U}_{0k}^*]$ and $[\boldsymbol{V}_{0k}^*]$, and $\{\hat{\boldsymbol{\phi}}_0^*\}$ and $\{\hat{\boldsymbol{q}}_0^*\}$ according the known boundary conditions, respectively. For degrees of freedom with prescribed temperature, the related elements in $\{\hat{\boldsymbol{\phi}}_0^*\}$ are selected for $\{\boldsymbol{d}_0^*\}$, and the corresponding rows of in $[\boldsymbol{U}_{0k}^*]$ are selected for $[\boldsymbol{A}_{0k}^*]$; otherwise, elements in $\{\hat{\boldsymbol{q}}_0^*\}$ are selected for $\{\boldsymbol{d}_0^*\}$, and the corresponding rows in $[\boldsymbol{V}_{0k}^*]$ are selected for $[\boldsymbol{A}_{0k}^*]$.

The set of Eq. (15) is solved for the unknown parameters $\boldsymbol{x}$ by the standard Gauss elimination solver, and then, by back-substitution into Eqs. (6), (7), (11) and (12), the boundary unknowns are obtained either on the interfaces or the external boundary surfaces. As demonstrated, the multi-domain HdBNM is a boundary-only meshless approach. No boundary elements are used for either interpolation or integration purposes. Therefore, it may alleviate the discretization difficulty to a large extent.

As a preliminary step of our study, we have employed the above multi-domain model to study the temperature distribution and heat flux concentration within or near the CNT by a RVE including single straight and sinusoidal CNT [24]. The concept of RVE has been widely used for conventional fiber-reinforced composites at the micro-scale [36]. Chen and Liu [37] applied it for the study of the CNT-based composites for their mechanical properties. Fisher et al. [38,39] analyzed the effects of the CNT waviness on the effective Young's modulus of the composites using an RVE containing a curved CNT. We have also studied the impact of the CNTs alignment on the equivalent thermal

Author's personal copy

properties [40]. It has been demonstrated that the equivalent thermal properties are strongly dependent on the CNTs alignment.

3. Simplified mathematical model for CNT composites

The computations using the multi-domain model have provided us some insights into the thermal properties of the composites. However, these computations are limited to relatively small scales, as only single or several but shorter CNTs were considered. When the number of CNTs included in the RVE is increased, the lengths of CNTs are reduced. This is because the total number of degrees of freedom of a problem that can be solved by the standard multi-domain solver within the available computer resources is limited to about 5000. In order to reduce the size scale of the linear system, we have proposed a simplified mathematical model for simulation of the CNT composites [26], by which the total number of degrees of freedom is reduced by nearly half. For the sake of completeness, the formulation development of this model is outlined in this section.

As demonstrated in [24,25], the unusually high heat conductivity of the CNTs in comparison with the polymer makes the temperature distribution within an individual CNT almost uniform. This feature allows us to simplify the modeling of the CNT-based composites. In the simplified model, only single domain, namely the polymer matrix is modeled. Each CNT is treated as a heat superconductor with one constant temperature constrained at its surface. A similar assumption can be found in a rigid-line inclusion model [41].

Using the HdBNM, the same Eqs. (6) and (7) in Section 2 for the polymer domain can be obtained. By combining Eqs. (6) and (7), we get

$$\begin{bmatrix} \boldsymbol{A}_{00} & \boldsymbol{A}_{01} & \cdots & \boldsymbol{A}_{0n} \\ \boldsymbol{U}_{10} & \boldsymbol{U}_{11} & \cdots & \boldsymbol{U}_{1n} \\ \vdots & \vdots & \ddots & \vdots \\ \boldsymbol{U}_{n0} & \boldsymbol{U}_{n1} & \cdots & \boldsymbol{U}_{nn} \end{bmatrix} \begin{Bmatrix} \boldsymbol{x}_0 \\ \boldsymbol{x}_1 \\ \vdots \\ \boldsymbol{x}_n \end{Bmatrix} = \begin{Bmatrix} \boldsymbol{H}_0\boldsymbol{d}_0 \\ \boldsymbol{H}_1\hat{\boldsymbol{\phi}}_1 \\ \vdots \\ \boldsymbol{H}_n\hat{\boldsymbol{\phi}}_n \end{Bmatrix}, \tag{16}$$

where each row of sub-matrices $[\boldsymbol{A}_{0k}]$, $k = 0, 1, \ldots, n$, is supplied identically from that in $[\boldsymbol{U}_{0k}]$ or $[\boldsymbol{V}_{0k}]$ according to the boundary condition at the corresponding node, and the corresponding term of $\{\boldsymbol{d}_0\}$ comes from $\{\hat{\boldsymbol{\phi}}_0\}$ or $\{\hat{\boldsymbol{q}}_0\}$.

Further, suppose that m_k nodes are located at the interface of kth nanotube with the polymer, and a constant temperature ϕ_c^k is prescribed, namely

$$\{\boldsymbol{\phi}_k\} = \{\mathbf{1}\}_k \phi_c^k, \tag{17}$$

where $\{\hat{\boldsymbol{\phi}}_k\}$ are the nodal values of temperature at the interface; $\{\mathbf{1}\}_k$ is a column vector of m_k dimensions with all the elements equal to 1.

On the other hand, the law of conservation of energy states that, for steady-state heat conduction, the rate of thermal energy flowing into a CNT must equal that flowing out. Thus, the following relationship can be imposed on the surface of the kth CNT:

$$\int_{C_k} q \mathrm{d}\Gamma = 0, \tag{18}$$

where C_k represents the outer surface of the kth CNT. Substituting Eq. (2) into (18) and omitting the common factor κ, we get

$$\sum_{J=1}^{N} \int_{C_k} \frac{\partial \phi_J^s}{\partial n} \mathrm{d}\Gamma x_J = 0. \tag{19}$$

In Eq. (19), C_k is a closed surface. The following integral identity holds [42]

$$\int_{C_k} \frac{\partial \phi_J^s}{\partial n} \mathrm{d}\Gamma = \begin{cases} 1, & \forall s_J \in C_k, \\ 0, & \forall s_J \notin C_k. \end{cases} \tag{20}$$

Inserting Eq. (17) into Eq. (16) and appending Eq. (19), we obtain the final set of algebraic equations system which can uniquely determine the unknown parameter $\boldsymbol{x}$.

$$\begin{bmatrix} \boldsymbol{A}_{00} & \boldsymbol{A}_{01} & \cdots & \boldsymbol{A}_{0n} & \mathbf{0} & \cdots & \mathbf{0} \\ \boldsymbol{U}_{10} & \boldsymbol{U}_{11} & \cdots & \boldsymbol{U}_{1n} & -H_1\{\mathbf{1}\}_1 & \cdots & \mathbf{0} \\ \mathbf{0} & \{\mathbf{1}\}_1^{\mathrm{T}} & \cdots & \mathbf{0} & \mathbf{0} & \cdots & \mathbf{0} \\ \vdots & \vdots & \ddots & \vdots & \vdots & \ddots & \vdots \\ \boldsymbol{U}_{n0} & \boldsymbol{U}_{n1} & \cdots & \boldsymbol{U}_{nn} & \mathbf{0} & \cdots & -\boldsymbol{H}_n\{\mathbf{1}\}_n \\ \mathbf{0} & \mathbf{0} & \cdots & \{\mathbf{1}\}_n^{\mathrm{T}} & \mathbf{0} & \cdots & \mathbf{0} \end{bmatrix} \times \begin{Bmatrix} \boldsymbol{x}_0 \\ \boldsymbol{x}_1 \\ \vdots \\ \boldsymbol{x}_n \\ \boldsymbol{\phi}_c^1 \\ \vdots \\ \boldsymbol{\phi}_c^n \end{Bmatrix} = \begin{Bmatrix} \boldsymbol{H}_0\boldsymbol{d}_0 \\ \mathbf{0} \\ 0 \\ \vdots \\ \mathbf{0} \\ 0 \end{Bmatrix}. \tag{21}$$

The set of Eq. (21) is solved for the unknown parameters $\boldsymbol{x}$ and ϕ_c^k, then, by back-substitution into Eqs. (6) and (7), the boundary unknowns are obtained either on the interfaces or the external boundary surfaces.

The simplified mathematical model has been rigorously validated through numerical examples [25]. It is also verified that, for a composite material, when the ratio of heat conductivity between the inclusions and the matrix is bigger than 2000, the simplified model is adequate for evaluating the overall thermal properties of composite with sufficient accuracy. As the lowest value of the ratio of heat conductivity between CNT and a polymer, ever reported in the literature, is much higher than 2000, the CNTs can be treated, without loss of accuracy, as a heat superconductor

Author's personal copy

in the mathematical model of the composite heat transfer analysis.

4. The Fast Multipole Method

The size of the coefficient matrix in Eq. (21) is dominated by sub-matrices $[\boldsymbol{A}_{0k}]$ and $[\boldsymbol{U}_{ki}]$, $k = 1,\ldots n$, $i = 0, 1,\ldots n$. Since these sub-matrices are unsymmetrical and fully populated, solving Eq. (21) by an iterative solver requires $O(N^2)$ operations. In this paper, we use the restarted preconditioned GMRES [43] to solve the equation. The most time-consuming aspect of an iterative method when employed for solving a system of linear equations is the matrix–vector product in each iteration step. Taking an iteration vector $\mathbf{x}'$ into account, the product of a row of the coefficient matrix in Eq. (21) and the guess vector $\mathbf{x}'$ can be expressed as one of the following four sums:

$$\sum_{J=1}^{N} \int_{\Gamma_I} \phi_J^s v_I(Q) x'_J \mathrm{d}\Gamma, \tag{22}$$

$$\sum_{J=1}^{N} \int_{\Gamma_I} -\kappa \frac{\partial \phi_J^s}{\partial n} v_I(Q) x'_J \mathrm{d}\Gamma, \tag{23}$$

$$\sum_{J=1}^{N} \int_{\Gamma_I} \phi_J^s v_I(Q) x'_J \mathrm{d}\Gamma + \phi_c^k \sum_{J}^{m_k} H_{IJ}, \tag{24}$$

$$\sum_{J}^{m_k} x_J^k. \tag{25}$$

Sums (22) and (23) are related to a node located on the external boundary and prescribed with temperature and normal flux, respectively. Sum (24) is related to a node located at the interface of the kth CNT with the polymer domain, and Expression (25) to the kth uniform temperature constraint.

The computational costs for the second term in Sums (24) and (25) are trivial, and can be ignored. However, direct implementation of Sums (22) and (23) gives an $O(N^2)$ algorithm. When N grows large, this algorithm leads to rapid exhaustion of computer resources like memory, disk space, and CPU time, which limits the number of CNTs that can be included in an RVE. In this work, we use FMM to reduce the complexity of these summations. The FMM is powerful but also complicated in implementation. In the following, we briefly list the main ideas of the FMM for accelerating summation (22) as a similar idea can be easily applied to Sum (23). A complete description of combination of FMM and HdBNM can be found in Ref. [35].

Instead of treating interactions with each of the distant nodes individually, the FMM computes cell–cell interactions, thus achieves an $O(N)$ complexity algorithm. Consider two cells C_a and C_b: C_a contains N_a nodes and C_b contains N_b nodes. The computational complexity of a standard algorithm for the mutual interactions between the two groups is of order $O(N_a \times N_b)$ (Fig. 1a), while using the

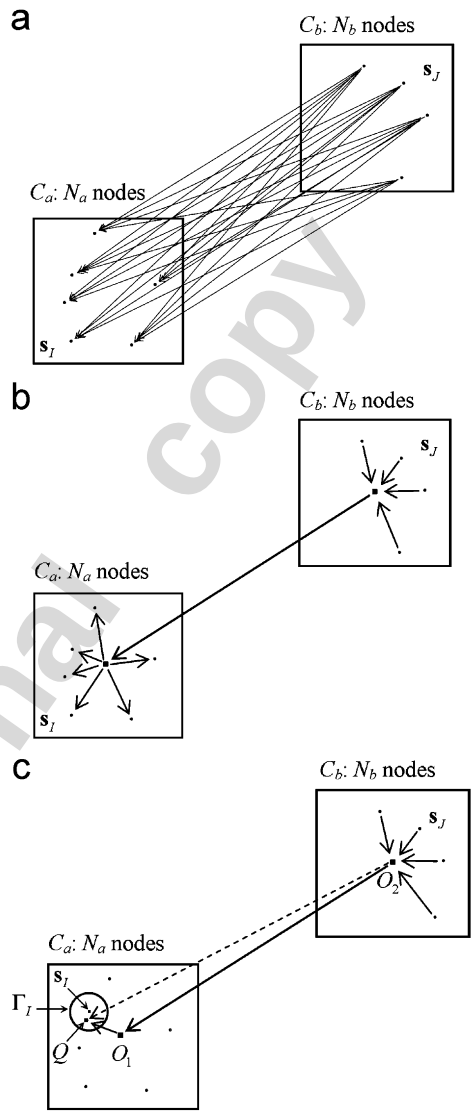

Fig. 1. Interaction between two cells.

cell–cell strategy, it is reduced to $O(N_a + N_b)$ (Fig. 1b). To conduct the cell–cell interaction computation, the fundamental solution in Eq. (3) is expanded in terms of solid harmonic series:

$$\phi_J^s = \frac{1}{4\pi\kappa} \frac{1}{r(Q, \mathbf{s}_J)} = \frac{1}{4\pi\kappa} \sum_{n=0}^{\infty} \sum_{m=-n}^{n} \overline{S_{n,m}}(\overrightarrow{O_2Q}) R_{n,m}(\overrightarrow{O_2\mathbf{s}_J}) \tag{26}$$

for $|\overrightarrow{O_2Q}| > |\overrightarrow{O_2\mathbf{s}_J}|$, in which O_2 represents the center of C_2 (Fig. 1c), $R_{n,m}$ and $S_{n,m}$ are solid harmonic functions defined in Ref. [44], and $\overline{(\,)}$ means the complex conjugate. Substituting (26) into (22) for summation over the nodes included in C_b, we obtain

$$\sum_{J=1}^{N_b} \int_{\Gamma_I} \phi_J^s v_I(Q) x'_J \mathrm{d}\Gamma = \sum_{n=0}^{\infty} \sum_{m=-n}^{n} \int_{\Gamma_I} \frac{1}{4\pi\kappa} \overline{S_{n,m}}(\overrightarrow{O_2Q}) v_I(Q) d\Gamma M_{n,m}(O_2), \tag{27}$$

Author's personal copy

in which,

$$M_{n,m}(O_2) = \sum_{J=1}^{N_b} R_{n,m}(\overrightarrow{O_2 s_J}) x'_J \tag{28}$$

is called *multipole moments* for given m and n.

The solid harmonic function $\overline{S_{n,m}}(O_2 Q)$ in Eq. (27) can be further expanded in terms of solid harmonics as [29,44]

$$\overline{S_{n,m}}(\overrightarrow{O_2 Q}) = \sum_{n'=0}^{\infty} \sum_{m'=-n'}^{n'} (-1)^{n'} R_{n',m'}(\overrightarrow{O_1 Q}) \overline{S_{n+n',m+m'}}(\overrightarrow{O_1 O_2}) \tag{29}$$

for $|\overrightarrow{O_1 O_2}| > 2|\overrightarrow{O_1 Q}|$, where O_1 is the center of C_a (Fig. 1c). Substituting (29) into (27), we arrive at

$$\sum_{J=1}^{N_b} \int_{\Gamma_I} \phi_J^s v_I(Q) x'_J \mathrm{d}\Gamma = \sum_{n'=0}^{\infty} \sum_{m'=-n'}^{n'} \int_{\Gamma_I} \frac{1}{4\pi\kappa} R_{n',m'}(\overrightarrow{O_1 Q}) v_I(Q) \mathrm{d}\Gamma L_{n',m'}(O_1), \tag{30}$$

where

$$L_{n',m'}(O_1) = \sum_{n=0}^{\infty} \sum_{m=-n}^{n} (-1)^{n'} \overline{S_{n+n',m+m'}}(\overrightarrow{O_1 O_2}) M_{n,m}(Q_2). \tag{31}$$

Eq. (31) is called *multipole to local* translation, which transforms the multipole moments of C_b to the local moments of C_a.

In the above development, the multipole expansions are used to separate the source and target points in the fundamental solution and the pair of points in the solid harmonic functions, so that the multipole moments and local moments are related only to the cells, respectively. Therefore, these moments can be calculated independently and can be aggregated into ones to represent potentials of ever lager groups of nodes. Moreover, once calculated, they can be reused for all other cell–cell interactions.

Besides the multipole to local translation, the FMM also uses *multipole to multipole* and *local to local* translations, and a hierarchical decomposition of space, represented by a tree structure, that rationally partitions the computation domain into areas that are suitably distant from each other. By the translation operators, the multipole and local moments are orchestrated in the tree structure in a recursive way. It consists of two basic steps: the *upward pass* and the *downward pass*. During the upward pass, multipole moments are accumulated from leaves to the root of the tree. During the downward pass, local moments are distributed from the root to the leaves. In practical computation, the infinite series in the expansions and translations are truncated after p terms. It has been found that for $p = 10$, these expansions and translations are sufficiently accurate for most problems. As p is a small constant, the computational complexity for computing Sums (22) and (23) is proportional to N. For full details of fast multipole HdBNM refer to [35].

4.1. Accuracy validation of FMM

The accuracy of FMM is determined by the number of terms, p, used in the multipole expansions. One of the advantages of FMM is that it bounds the error analytically. As we can determine how many terms are required in a multipole expansion to achieve a certain guaranteed level of accuracy, the FMM can be arbitrarily accurate. In this section, we will examine the accuracy of the above-proposed method. An RVE with a sinusoidal CNT embedded is used in this study. Fig. 2 shows the geometry and dimensions. As there is no analytical solution existing for the simplified model, we consider the matrix domain, only, and impose Dirichlet boundary condition on all the surfaces, including cavity (the outer surface of the CNT), according to the following exact solution:

$$u = x^3 + y^3 + z^3 - 3yx^2 - 3xz^2 - 3zy^2, \tag{32}$$

then solve the problem using Eqs. (6) and (7). This set up cannot actually check the accuracy of the simplified model combined with FMM but the FMM, only. The simplified mathematical model has been rigorously validated in [25]. The relative error is evaluated over all the boundary nodes using a 'global' L_2 norm error defined as

$$e = \frac{1}{|q|_{\max}} \sqrt{\frac{1}{N} \sum_{i=1}^{N} (q_i^{(e)} - q_i^{(n)})^2}, \tag{33}$$

where $|q|_{\max}$ is the maximum nodal value of normal flux, the superscripts (e) and (n) refer to the exact and numerical solutions, respectively.

We have performed computations for a variety of numbers of nodes uniformly distributed on the inner and outer surfaces of the domain. We truncate all the infinite expansions after $p = 10$, set the maximum number of boundary nodes in a leaf box to be 60, and terminate the iteration when the relative error norm is less than 10^{-6}. All the computations in this paper, including that presented in the next section, are performed on a desktop computer with an Intel(R) Pentium(R) 4 CPU (1.99 GHz).

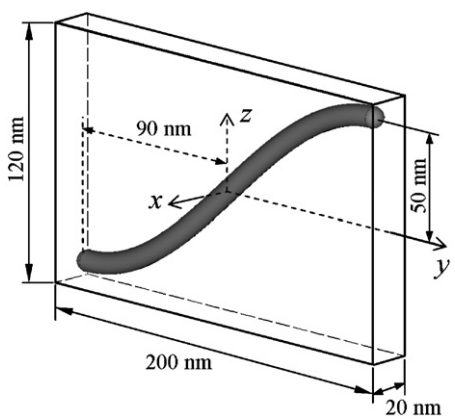

Fig. 2. An RVE including a sinusoidal CNT.

Author's personal copy

The relative errors as a function of the number of nodes used are presented in Fig. 3. The error with the coarsest nodes (5616 nodes) is 2.027%, while that with the finest nodes (151,724 nodes) is 0.4076%. With an increasing number of nodes, higher accuracy is obtained. The solution time is plotted against the number of nodes in Fig. 4, which clearly shows a nearly linear complexity of the developed algorithm. The high accuracy and efficiency for this example suggests that the proposed formulation and its FMM implementation are correct and effective. This example also demonstrates that the proposed method is capable of performing large-scale computations. In the next section, we will employ it for advanced analysis of the CNT-based composites.

5. Thermal studies by the simplified model and FMM

5.1. Middle-scale studies

A rectangular RVE is employed with the dimensions shown in Fig. 5. Based on the simplified mathematical model, the CNTs are treated as cavities, which are identical to the outer surfaces of the CNTs. Constant temperatures are constrained at each of the cavity surfaces. The radii of CNTs ($R = 5$ nm) are kept constant in all the following examples, while their length and shapes, together with the number of CNTs and their alignments, varies for different examples. The heat conductivity, κ^p, used for the polymer (polycarbonate) is 0.37 W/m K. Uniform temperatures of 300 and 200 K are imposed at the two end faces of the RVE, respectively, and heat flux free at other four side faces. This boundary condition set allows us to estimate equivalent heat conductivity of the composite in the axial direction. Using Fourier's law, the formula for equivalent heat conductivity can be written as

$$\kappa = -\frac{qL}{\Delta\phi}, \tag{34}$$

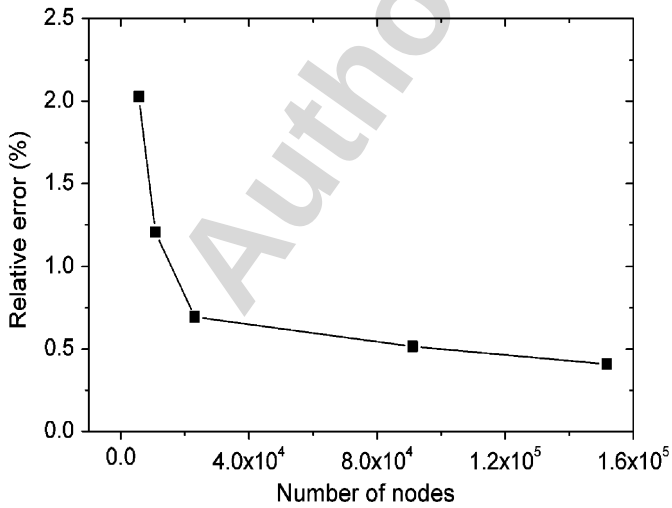

Fig. 3. Relative error for normal flux.

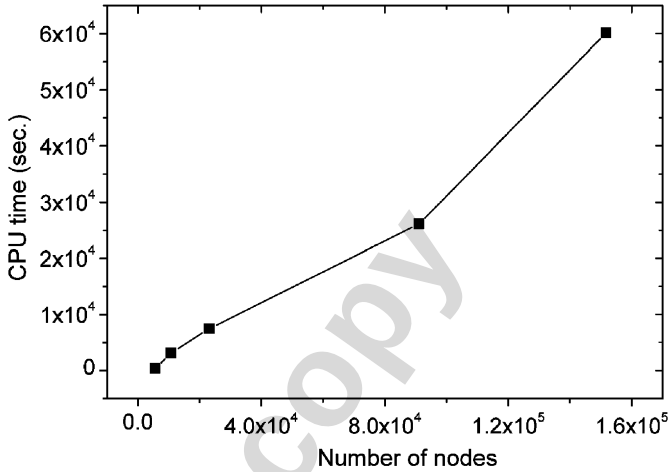

Fig. 4. CPU time for solving system equation.

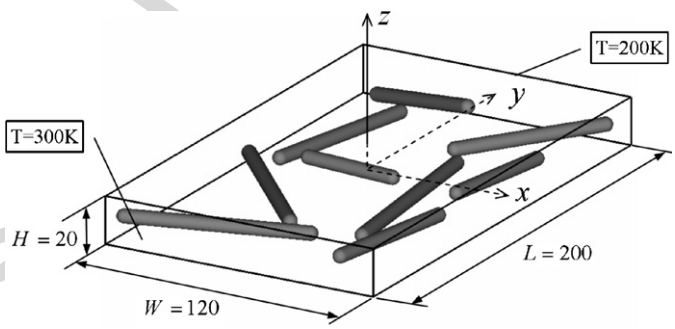

Fig. 5. Dimensions of a nanoscale RVE.

where κ represents the heat conductivity, q is the average value of normal flux at the two end face, obtained by HdBNM, L is the length of the RVE in the axial direction and $\Delta\phi$ the temperature difference between the two end faces.

Twelve RVEs containing different numbers of CNTs with different shapes, alignments, have been considered. These RVEs are sorted into three groups according to their shape and alignment, and presented in Figs. 6–8. The first group consists of RVEs including straight CNTs with parallel alignment. The length of these CNTs is 195 nm. In the RVEs of the second group, two more vertically aligned CNTs are added near the two end faces. The third group includes RVEs with curved CNTs embedded. Results of our experiments are summarized in Table 1. In the table, the first column lists the number of the RVE, the second column lists the volume fraction of CNT, the third column lists the calculated effective heat conductivity, and the fourth column lists the ratio of the effective heat conductivity to that of the polymer. To assess the enhancement effectiveness, we use as the criterion the ratio of the effective heat conductivity to the volume fraction, which is presented in the fifth column.

Results in Table 1 show that, for RVEs of group 1, as the number of CNTs included in the RVE increases, the

Author's personal copy

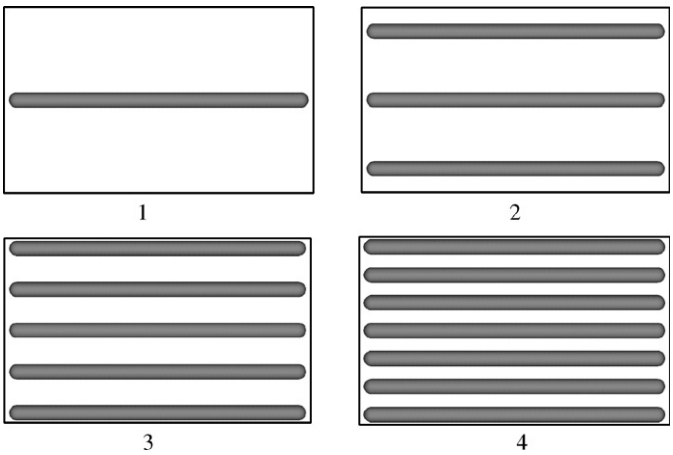

Fig. 6. RVEs including straight CNTs, alignment 1.

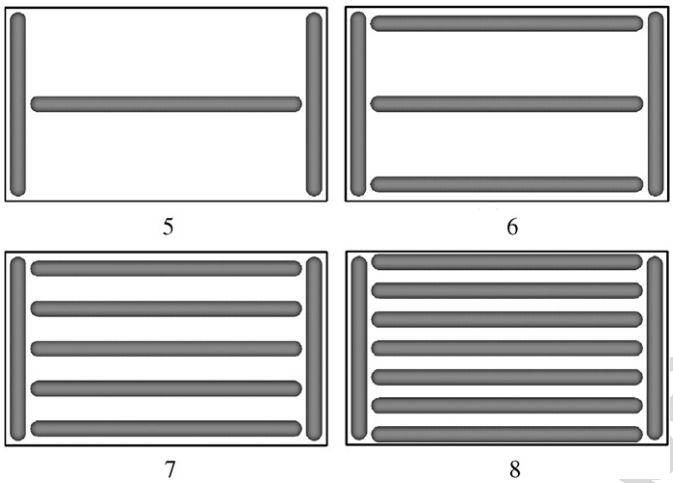

Fig. 7. RVEs including straight CNTs, alignment 2.

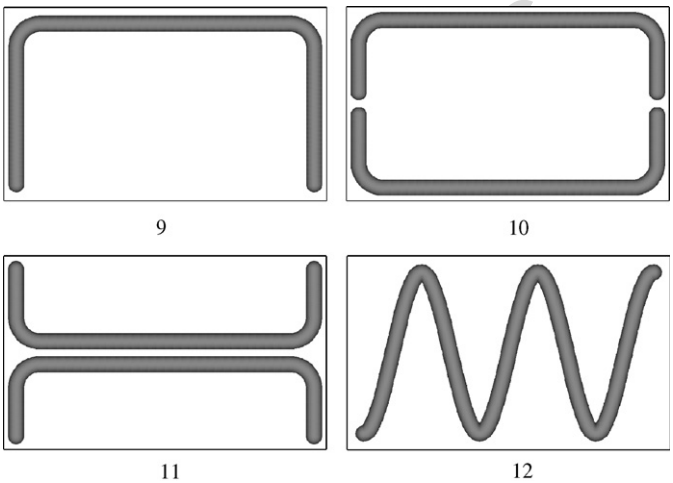

Fig. 8. RVEs including curved CNTs, alignment 3.

effective heat conductivity increases, while the effectiveness of enhancement decreases. Results for RVEs of group 2 are quite similar. However, their enhancements are smaller than that obtained by RVEs of group 1. It is interesting to note that the case (9) gives the highest values of both the effectiveness of enhancement and the effective heat conductivity, which is much higher than that obtained for models with straight CNTs. The effective heat conductivity is 21 times that of the polymer.

Table 1
Effective heat conductivities for middle-scale RVEs

RVE	CNT volume fraction, v (%)	Effective conductivity, κ (W/m K)	Reinforcement κ/κ^p	Effectiveness κ/v
(1)	3.136	1.646	4.5	52.49
(2)	6.272	3.780	10.2	40.18
(3)	9.408	5.079	13.7	32.39
(4)	15.68	6.114	16.5	27.85
(5)	6.381	1.334	3.6	20.91
(6)	11.84	2.294	6.2	19.37
(7)	17.29	2.868	7.6	16.59
(8)	22.74	3.138	8.5	13.80
(9)	6.198	7.680	21	123.9
(10)	8.796	7.155	19	81.34
(11)	8.796	7.179	19	81.62
(12)	9.010	1.941	5.2	21.54

5.2. Large-scale studies

In this section, the RVE used in the previous section is enlarged such that $L = 630\,\text{nm}$, $H = 385\,\text{nm}$ and $W = 100\,\text{nm}$. Except the number and geometries of CNTs embedded in the RVE, the rest parameters including the boundary condition are kept the same as in the previous section.

Eight RVEs containing different numbers of CNTs with different shapes, alignments, have been elaborately built, which are presented in Fig. 9. RVE (13) contains 135 identical CNTs, of which the geometry and dimensions are the same as that in the RVEs shown in Fig. 6. RVE (14) and (15) are built from RVE (13) by "randomly" modifying the location in y direction and orientation of each CNT slightly, respectively. The word randomly is quoted because the variations of location and orientation are limited to such an extent that each CNT remains in a local box that includes the CNT to avoid contact of the CNTs. RVE (16) includes 45 curved CNTs of sinusoidal shape. The wave number and amplitude of the sinusoidal curves for the shapes of the CNTs vary from one to another to make this RVE more realistic looking. RVE (17) includes 45 identical CNTs of "C" shape, which are duplicated from the CNT in RVE (9) shown in Fig. 8. RVE (18) contains single long CNT of "C" shape, and in RVE (19), this long CNT is duplicated two times. In RVE (20), we deliberately build a very long and curved CNT. We expect this RVE will give the best result of heat conductivity.

In Table 2, we summarize the computational results for these RVEs. As our expectation, the best results are obtained from case (20), which gives the highest values for

Personal copy

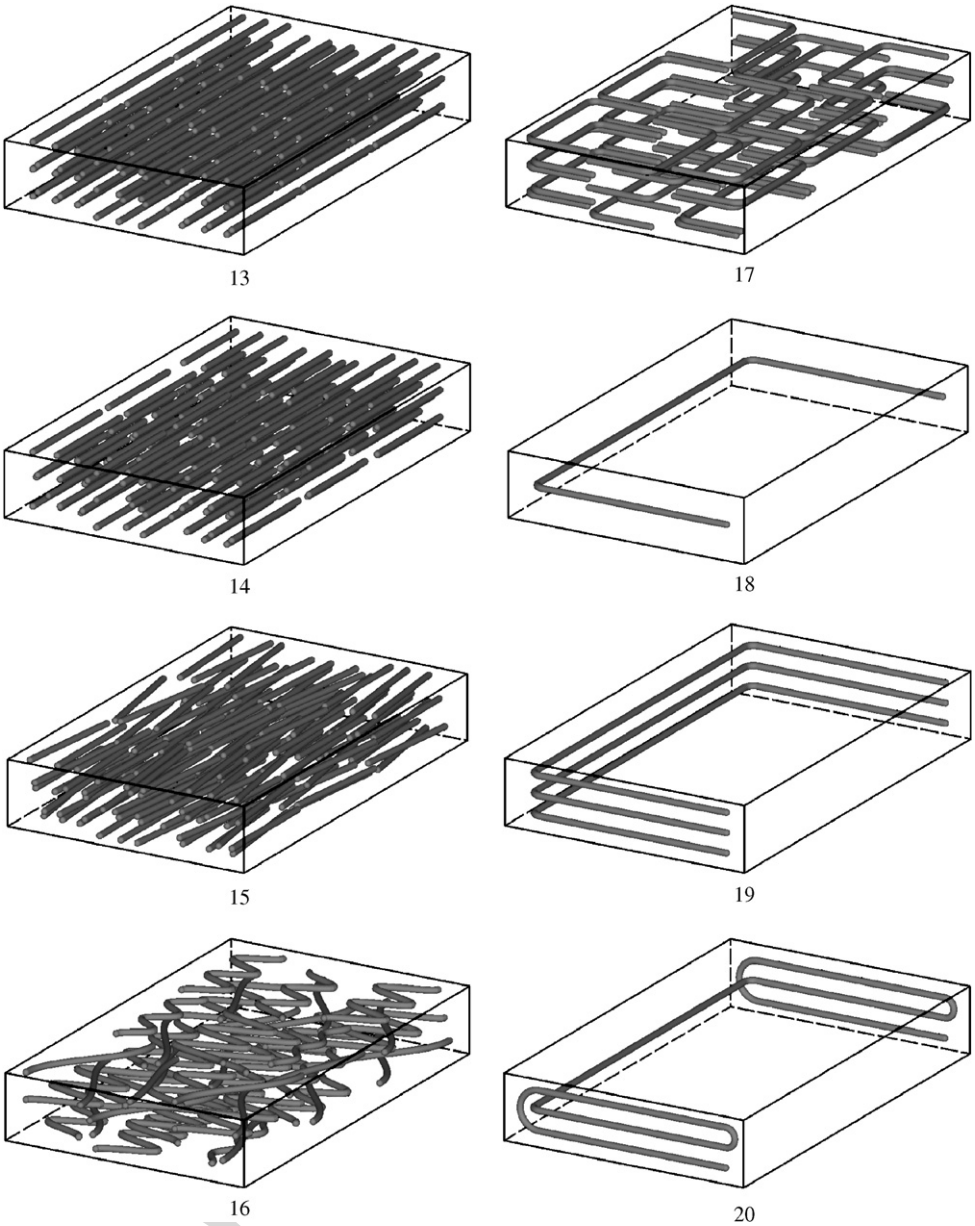

Fig. 9. Nanoscale RVEs containing various nanotubes: (13) uniformly located 135 CNTs; (14) "Randomly" located 135 CNTs; (15) "Randomly" oriented 135 CNTs; (16) "Randomly" located 45 curved CNTs; (17) forty-five CNTs of "C" shape; (18) single CNT of "C" shape; (19) three CNTs of "C" shape; (20) single long and curved CNT.

Table 2
Effective heat conductivities for large-scale RVEs

RVE	CNT volume fraction, v (%)	Effective conductivity, κ (W/m K)	Reinforcement, κ/κ^p	Effectiveness, κ/v
(13)	8.4	3.746	10.1	44.71
(14)	7.7	2.668	7.2	35.55
(15)	8.4	3.470	9.4	41.41
(16)	4.8	1.717	4.6	36.00
(17)	5.5	6.319	17.1	114.5
(28)	0.40	4.868	13.2	1218
(19)	1.2	11.15	30.1	929.9
(20)	0.88	11.76	31.8	1337

both the effective heat conductivity (= 11.76 W/m K) and the ratio κ/v (= 1337). The heat conductivity obtained from case (20) is close to that of metals. That means, with longer CNTs, it is possible to make a CNT-based composite with the effective heat conductivity comparable to or higher than metals'. Case (19) gives the second highest value of heat conductivity (= 11.15 W/m K), very close to the best one, and the third highest value for the ratio κ/v (= 929.9). Case (18) gives the fourth highest value of heat conductivity (= 4.868 W/m K) and the second highest value for the ratio κ/v (= 1218). And case (17) gives the third highest value of heat conductivity (= 6.319 W/m K) and the fourth highest value for the ratio

κ/v (= 114.5). The common feature of these three RVEs is that all of them contain CNTs of "C" shape. Although they do not give the best results, considering the simplicity of geometry, we suggest the "C" shape is the best shape of CNTs for enhancing thermal properties of the composites.

By comparing the results for RVEs listed in Tables 1 and 2, we make the following observations:

1. The effective conductivities obtained for cases (13), (16) and (17) are very close to those for cases (2), (9) and (12), respectively. As RVEs (13), (16) and (17) can be considered approximately as periodic structures with RVEs (2), (9) and (12) being the cells of periodicity, respectively, the proximity between the results demonstrates that the global behavior of a periodic structure can be characterized by a single cell of periodicity of the structure, and thus validates the applicability of the RVE method.
2. Numerical results obtained for cases (13)–(16) demonstrate that the CNT distribution, orientation, and especially, the waviness strongly affect the effective heat conductivity, while their influences on the ratio κ/v are less strong.
3. The ratios κ/v of cases (18) and (19) are nearly one order higher that of case (17), which suggests that CNT length is a decisive factor for the enhanced thermal property of the composite, while the volume fraction of CNT is much less important. The most effective way to increase the heat conductivity of the composite is to use longer CNTs to be embedded in the composite. The same conclusion can be made by comparing cases (18) and (13), where the case (18) gives higher value of conductivity with a long CNT but extremely less volume fraction.

5.3. Sensitive study on CNT's curvature

Micrographs of CNT composites show that the embedded CNTs exhibit significant curvature within the polymer [38,39]. In the previous section, it is shown that the shape and curvature of the embedded CNT greatly influence the effective heat conductivity of the CNT composites. However, the degree of the influence has been unclear. Sinusoidal and spiral shapes are the typically observed curvatures of the embedded CNTs. In this section, we examine the impact of the curvature of CNTs on the effective thermal properties of the composites. Dimensions of two RVEs used in this study are presented in Figs. 10 and 11. The outer dimensions: $180 \times 180 \times 530$ are the same for both RVEs, while the shapes of the CNTs embedded are different. The RVE shown in Fig. 10 includes CNTs of sinusoidal shape, while the RVE in Fig. 11 contains spiral CNTs. Dimensions of the sinusoidal CNT and the spiral CNT are given in Figs. 10b and 11b, respectively. Both RVEs include 27 uniformly arrayed identical CNTs with a dislocation of 30 nm in y direction

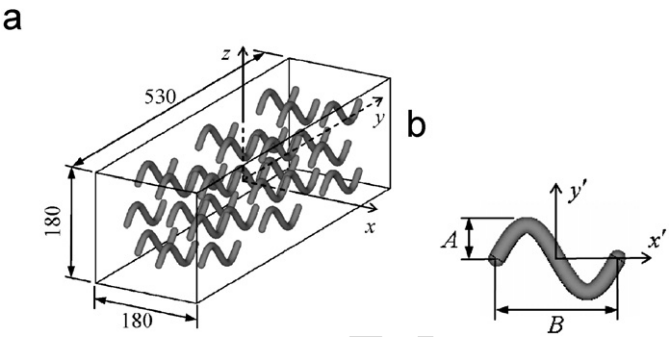

Fig. 10. RVE containing sinusoidal CNTs.

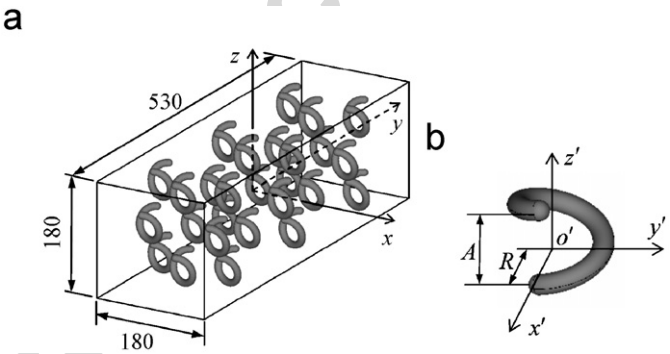

Fig. 11. RVE containing spiral CNTs

between the neighboring rows. In this study, we will keep the length of each CNT constant (= 120 nm), while change amplitude of the sinusoidal curve and the radius of the spiral curve from 20 to 0 nm. The total number of nodes used for each instance is 110,391. The boundary conditions are kept the same as in previous sections, uniform temperatures of 300 and 200 K are prescribed at the two end faces ($y = 265$ and -265), respectively, while all the rest faces are treated as flux free. Computations were performed for five sets of dimensions for each of the CNTs, namely, A or $R = 20$, 15, 10, 5, 0. The corresponding images of the RVEs are shown in Figs. 12 and 13.

The effective heat conduction as a function of the amplitude for the sinusoidal CNTs and the radius for the spiral CNTs is presented in Fig. 14. It is seen that the curvature of CNTs indeed has a strong impact on the overall thermal properties of the composites. For the sinusoidal CNTs, the effective heat conductivity obtained by the straight CNTs is 1.4 times that obtained by the sinusoidal CNTs with amplitude being 20 nm, while for the spiral CNTs, the RVE with straight CNTs embedded gives 2.2 times effective conductivity that obtained by the spiral CNTs of 20 nm radii. It can be also seen that, in all cases, the sinusoidal CNTs perform much better than the spiral CNTs. This observation is consistent with the physical interpretation. When the amplitude of sinusoidal curve equals to the radius of the spiral curve, a sinusoidal CNT spans a longer distance in the y direction than a spiral CNT

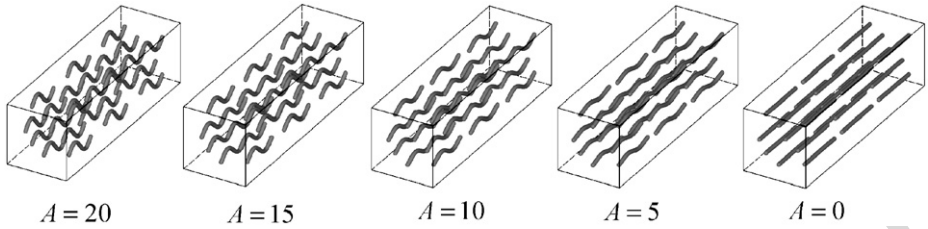

Fig. 12. RVEs containing sinusoidal CNTs with various amplitudes.

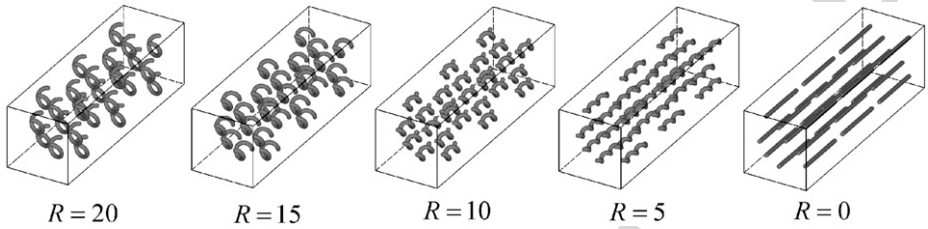

Fig. 13. RVEs containing spiral CNTs with various radii.

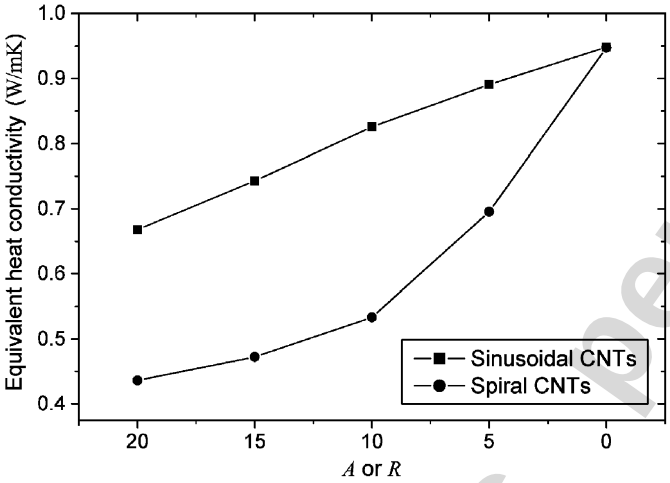

Fig. 14. Variation of effective heat conductivity with decreasing curvature of CNTs.

of the same length, therefore, the sinusoidal CNTs bridge a better heat conduction path which reduces the heat conduction resistance.

6. Discussions and conclusions

This paper presents an implementation of HdBNM combined with FMM to the heat conduction analysis in CNT-based composite material based on multi-domain model and a simplified mathematical model. The HdBNM is a meshless boundary-only method requiring discrete nodes located on bounding surfaces of the domain of interest, only. That greatly simplifies the pre-processing and discretization tasks and makes approach extremely useful, and more cost- and resources-effective than based on conventional FEM/BEM models. Numerical examples have demonstrated that the fast multipole HdBNM is an accurate and effective algorithm and has promising applications in large-scale analysis of CNT composites, especially concerning the complex geometries of the CNTs.

Mathematical models presented in the paper rely on continuum mechanics principles and do not account for quantum effects. However, the continuum-based model seems to be so far the only feasible one for performing simulations of nanocomposites behavior and properties at practical/engineering level. How to address the quantum effects in a continuum or multi-scale model will be a challenging task that needs to be studied in the future. At current stage of research, the objective is to gain insight into the thermal property of the CNT composites through numerical simulation on RVEs of the composites that contain a large number of randomly scattered CNTs with various geometries, and find some new composites with optimal configurations of CNTs.

A variety of RVEs containing different numbers of CNTs, from small to large scales, have been studied in an attempt to investigate the influence of CNT length, distribution, orientation and volume fraction on the overall thermal properties of the composites. We found that all the above factors have strong impact on the overall properties of the composites. However, the length of the individual CNTs is substantially decisive for enhancing the thermal properties of the composite, while the volume (or weight) fraction of CNT is less important. For a specific length of CNTs, the degree of improvement for effective heat conductivity is not proportional to the volume fraction of CNT. With increasing the volume fraction, the effectiveness of enhancement of the CNTs decreases.

Increasing the lengths of CNTs that embedded in a polymer system is the most effective way to enhance the heat conductivity of the system. However, this has received little attention. In literatures of both numerical and experimental studies on CNT composites, researchers often assess the enhanced properties in terms of volume (or weight) fraction of the CNTs, and seldom compare the

Author's personal copy

enhancement for CNTs of different lengths. In our study, we found that substantially higher effective heat conductivity can be attained with a small fraction of long CNTs than with a large fraction of short CNTs. Moreover, from the point view of practical fabrication of CNT composite, it is easier to achieve uniform dispersion of CNTs into the polymer with low fractions of CNT.

A critical issue that has been examined is the impact of the shape of CNTs on the effective thermal properties of the composites. RVEs containing CNTs with various shapes are computed and compared. Results demonstrate that the effective heat conductivity is strongly dependent on the embedded CNTs' geometries. For a specific length, the "C" shape is suggested to be the most effective shape for thermal property enhancement. Future work will focus on optimizing the dimensions of the "C" shape CNT with some specific lengths.

The effects of the CNT curvature on the effective conductivity were also investigated. It is found that the CNT curvature indeed reduces the effective enhancement when compared with straight CNTs. The reason for a curved CNT reduces the effective enhancement is that it decreases the spanned distance along its axial dimension. This mechanism of reduction of enhancement is different from that in elastostatic case [38]. In the sensitive studies on CNT curvature, when we kept the spanned distance along its axial dimension constant while changed the curvature and the length of the CNT(s), results showed that the effective heat conductivity was only slightly affected by the waviness of the CNT [24].

Acknowledgments

The support of Japan Society for the Promotion of Sciences (JSPS) and Shinshu University, Nagano, Japan, is gratefully acknowledged. Parts of this work were financially supported by the Grant-in-Aid for JSPS Fellows No. 17_05075.

References

[1] Thostenson ET, Ren ZF, Chou TW. Advances in the science and technology of carbon nanotubes and their composites: a review. Compos Sci Technol 2001;61:1899–912.
[2] Endo M, Kim YA, Hayashi T, Nishimura K, Matushita T, Miyashita K, et al. Vapor-grown carbon fibers (VGCFs): basic properties and their battery applications. Carbon 2001;39:1287–97.
[3] Ruo RS, Lorents DC. Mechanical and thermal properties of carbon nanotubes. Carbon 1995;33(7):925–30.
[4] Lu JP. Elastic properties of single and multilayered nanotubes. J Phys Chem Solids 1997;58(11):1649–52.
[5] Ren ZF, Huang ZP, Xu JW, Wang JH, Bush P, Siegal MP, et al. Synthesis of large arrays of well-aligned carbon nanotubes on glass. Science 1998;282(5391):1105–7.
[6] Hone J, Whitney M, Piskoti C, Zettl A. Thermal conductivity of single-walled nanotubes. Phys Rev B 1999;59(4):2514–6.
[7] Yi W, Lu L, Zhang DL, Pan ZW, Xie SS. Linear specific heat of carbon nanotubes. Phys Rev B 1999;59:9015–8.
[8] Kim P, Shi L, Majumdar A, McEuen Pl. Thermal transport measurements of individual multiwalled nanotubes. Phys Rev Lett 2001;87:215502–11.
[9] Berber S, Kown YK, Tomanek D. Unusually high thermal conductivity of carbon nanotubes. Phys Rev Lett 2000;84(20): 4613–7.
[10] Osman MA, Srivastava D. Temperature dependence of the thermal conductivity of single-wall carbon nanotubes. Nanotechnology 2001;12(1):24.
[11] Che J, Cagin T, Goddard III WA. Thermal conductivity of carbon nanotubes. Nanotechnology 2000;11:65–9.
[12] Qian D, Dickey EC, Andrews R, Rantell T. Load transfer and deformation mechanisms in carbon nanotube polystyrene composites. Appl Phys Lett 2000;76(20):2868–70.
[13] Biercuk MJ, Llaguno MC, Radosavljevic M, Hyun JK, Johnson AT, Fischer JE. Carbon nanotube composites for thermal management. Appl Phys Lett 2002;80(15):2767–9.
[14] Liu YJ, Nishimura N, Otani Y. Large-scale modeling of carbon-nanotube composites by a fast multipole Boundary Element Method. Comput Mater Sci 2005;34:173–87.
[15] Sohlberg K, Sumpter BG, Tuzun RE, Noid DW. Continuum methods of mechanics as a simplified approach to structural engineering of nanostructures. Nanotechnology 1998;9(1):30–6.
[16] Zhang JM, Yao ZH, Li H. A hybrid boundary node method. Int J Numer Methods Eng 2002;53:751–63.
[17] Zhang JM, Yao ZH. Meshless regular hybrid boundary node method. Comput Model Eng Sci 2001;2:307–18.
[18] Zhang JM, Yao ZH, Tanaka M. The meshless regular hybrid boundary node method for 2-D linear elasticity. Eng Anal Bound Elements 2003;27:259–68.
[19] Zhang JM, Yao ZH. Analysis of 2-D thin structures by the meshless regular hybrid boundary node method. Acta Mech Sin 2002; 15:36–44.
[20] Zhang JM, Tanaka Masa, Matsumoto T. Meshless analysis of potential problems in three dimensions with the hybrid boundary node method. Int J Numer Methods Eng 2004;59:1147–60.
[21] Chen W. Symmetric boundary knot method. Eng Anal Bound Elements 2002;26:489–94.
[22] Chen W. Meshfree boundary particle method applied to Helmholtz problems. Eng Anal Bound Elements 2002;26:577–81.
[23] Chen W, Hon YC. Numerical convergence of boundary knot method in the analysis of Helmholtz, modified Helmholtz, and convection–diffusion problems. Comput Methods Appl Mech Eng 2003;192: 1859–75.
[24] Zhang JM, Tanaka Masa, Matsumoto T, Guzik A. Heat conduction analysis in bodies containing thin-walled structures by means of HdBNM with an application to CNT-based composites. JSME Int J Ser A: Solid Mech Mater Eng 2004;47:181–8.
[25] Zhang JM, Tanaka Masa, Matsumoto T. A simplified approach for heat conduction analysis of CNT-based nano-composites. Comput Methods Appl Mech Eng 2004;193:5597–609.
[26] Rokhlin V. Rapid solution of integral equations of classical potential theory. J Comput Phys 1985;60:187–207.
[27] Greengard L, Rokhlin V. A fast algorithm for particles simulations. J Comput Phys 1987;73:325–48.
[28] Greengard L, Rokhlin V. A new version of the Fast Multipole Method for the Laplace equation in three dimensions. Acta Numer 1997:229–69.
[29] Greengard L. The rapid evaluation of potential fields in particle systems. Cambridge: MIT Press; 1988.
[30] Yoshida K, Nishimura N, Kobayashi S. Application of fast multipole Galerkin boundary integral equation method to elastostatic crack problems in 3D. Int J Numer Methods Eng 2001;50: 525–47.
[31] Nishida T, Hayami K. Application of the Fast Multipole Method to the 3D BEM analysis of electron guns. In: Marchettia M, Brebbia CA, Aliabadi MH, editors. Boundary elements XIX. Computational Mechanics Publications; 1997. p. 613–22.

Author's personal copy

[32] Ying LX, Biros G, Zorin D. A kernel-independent adaptive fast multipole algorithm in two and three dimensions. J Comput Phys 2004;196:591–626.
[33] Liu YJ, Nishimura N, Otani Y, Takahashi T, Chen XL, Munakata H. A fast Boundary Element Method for the analysis of fiber-reinforced composites based on a rigid-inclusion model. J Appl Mech 2005;72:115–28.
[34] Nishimura N. Fast multipole accelerated boundary integral equation methods. Appl Mech Rev 2002;55:299–324.
[35] Zhang JM, Tanaka Masa, Endo M. The hybrid boundary node method accelerated by Fast Multipole Method for 3D potential problems. Int J Numer Methods Eng 2005;63:660–80.
[36] Hyer MW. Stress analysis of fiber-reinforced composite materials. Boston: McGraw-Hill; 1998.
[37] Chen XL, Liu YJ. Square representative volume elements for evaluating the effective material properties of carbon nanotube-based composites. Comput Mater Sci 2004;29(1):1–11.
[38] Fisher FT, Bradshaw RD, Brinson LC. Fiber waviness in nanotube-reinforced polymer composites—I: modulus predictions using effective nanotube properties. Compos Sci Technol 2003;63:1689–703.
[39] Bradshaw RD, Fisher FT, Brinson LC. Fiber waviness in nanotube-reinforced polymer composites—II: modeling via numerical approximation of the dilute strain concentration tensor. Compos Sci Technol 2003;63:1705–22.
[40] Tanaka Masa, Zhang JM, Matsumoto T. Multi-domain HdBNM for prediction of thermal properties of CNT composites. In: Proceedings of the first Asia-Pacific international conference on Computer Methods in Engineering JASCOME, 2003. p. 3–12.
[41] Nishimura N, Liu YJ. Thermal analysis of carbon-nanotube composites using a rigid-line inclusion model by the boundary integral equation method. Comput Mech 2004;35:1–10.
[42] Liu YJ, Rudolphi TJ. New identities for fundamental solutions and their applications to non-singular boundary element formulations. Comput Mech 1999;24:286–92.
[43] Saad Y, Schultz MH. GMRES: a generalized minimal residual algorithm for solving nonsymmetric linear system. J Sci Stat Comp 1986;7:856–69.
[44] Yoshida K. Applications of Fast Multipole Method to boundary integral equation method. PhD dissertation, Department of Global Environment Engineering, Kyoto University, 2001.

Author's personal copy